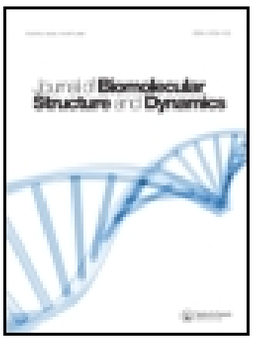

Taylor & Francis
Taylor & Francis Group

Journal of Biomolecular Structure and Dynamics

ISSN: 0739-1102 (Print) 1538-0254 (Online) Journal homepage: https://www.tandfonline.com/loi/tbsd20

Rational design of 9-vinyl-phenyl noscapine as potent tubulin binding anticancer agent and evaluation of the effects of its combination on Docetaxel

Shruti Gamya Dash, Charu Suri, Praveen Kumar Reddy Nagireddy, Srinivas Kantevari & Pradeep Kumar Naik

To cite this article: Shruti Gamya Dash, Charu Suri, Praveen Kumar Reddy Nagireddy, Srinivas Kantevari & Pradeep Kumar Naik (2020): Rational design of 9-vinyl-phenyl noscapine as potent tubulin binding anticancer agent and evaluation of the effects of its combination on Docetaxel, Journal of Biomolecular Structure and Dynamics, DOI: 10.1080/07391102.2020.1785945

To link to this article: https://doi.org/10.1080/07391102.2020.1785945

JOURNAL OF BIOMOLECULAR STRUCTURE AND DYNAMICS
https://doi.org/10.1080/07391102.2020.1785945

Rational design of 9-vinyl-phenyl noscapine as potent tubulin binding anticancer agent and evaluation of the effects of its combination on Docetaxel

Shruti Gamya Dash[a], Charu Suri[b], Praveen Kumar Reddy Nagireddy[c], Srinivas Kantevari[c] and Pradeep Kumar Naik[a]

[a]Centre of Excellence in Natural Products and Therapeutics, Department of Biotechnology and Bioinformatics, Sambalpur University, Sambalpur, Odisha, India; [b]Drug Discovery Research Centre, Translational Health Science and Technology Institute, Pali, Haryana, India; [c]Fluoro and Agrochemicals Division, CSIR-Indian Institute of Chemical Technology, Hyderabad, India

Communicated by Ramaswamy H. Sarma

ABSTRACT

Docetaxel (DOX) based combination therapy is a novel therapeutic strategy that attracts great interest in breast cancer treatment but its clinical utility got limited due to side effects. In contrast, noscapine, an antitussive drug showed antitumor activity against many cancers without any side effects that targets microtubules and attenuates its dynamic instability. In the quest for an increase in the anticancer activity of noscapine, we strategically designed a novel derivative, 9-vinyl phenyl noscapine (VPN), based on our *in silico* molecular docking and molecular dynamics simulation effort. Molecular docking of VPN and DOX onto microtubule revealed a docking score of −4.82 kcal/mol and −6.67 kcal/mol respectively, while the docking score of VPN was changed to −3.23 kcal/mol when it was docked onto the co-complex of tubulin-DOX. Further, the binding free energy ($\Delta G_{bind,PBSA}$) of VPN and DOX with tubulin showed −24.04 and −18.65 kcal/mol respectively, while the binding free energy of DOX was increased further in combination with VPN ($\Delta G_{bind,\ PBSA}$ was reduced to −21.41 kcal/mol), denoting combination effect of both ligands. The IC_{50} value amounted to 30.17 μM and 19.92 μM for VPN and 0.621 μM and 0.193 μM for DOX, respectively for 48 h and 72 h. The dose dependent cytotoxicity of DOX has been reduced considerably with the combination dose regimen of VPN. Further, the combine effect of both the agents improved the apoptotic cell death 28.5% compared to single agent treatment 5.71% and 10.5% for VPN and DOX, respectively. Both agents bind effectively to tubulin in single and in combination to interfere with cell cycle progression in G2/M transition. This study provides novel concept of combination treatment of DOX and VPN to amend efficiency in breast cancer treatment.

ARTICLE HISTORY
Received 2 April 2020
Accepted 16 June 2020

KEYWORDS
9-vinyl-phenyl noscapine; anti-tumor activity; combination drug therapy; molecular docking; molecular dynamics simulations; noscapine; noscapinoids; tubulin binding affinity

Introduction

Microtubule-targeting drugs such as taxol derivatives and vinca alkaloids have been powerful chemotherapeutic agents for the treatment of a variety of human cancers. However, primarily because of the poor solubility of these compounds, the clinical uses of these compounds have been somewhat cumbersome and expensive. In addition, these drugs are plagued with serious toxicity (particularly, peripheral neuropathies, gastrointestinal toxicity, myelosuppression, and immunosuppression) owing to their non-selective action (Rowinsky & Donehower, 1991; Kavanagh & Kudelka, 1993; Rowinsky, 1997; Theiss & Meller, 2000; Topp et al., 2000; Zhou et al., 2005). Despite all these challenges, taxol was approved by the FDA in 1996 for the treatment of breast and ovarian cancers. Nevertheless, the success of taxol in the management of aggressive breast and ovarian cancers gives an impetus to identify compounds that target microtubules, but are less toxic, bind differently to tubulin, more soluble in aqueous solutions, available orally and significantly effective either as single agents or can efficiently synergize with currently-available drugs such as docetaxel (at low doses). In quest of searching such molecule, noscapine (an opium alkaloid, non-narcotic, non-sedative, traditionally used for decades as an innocuous anti-cough medicine) was discovered (Ye et al., 1998). This class of compounds set themselves apart from currently-available anticancer drugs like *taxanes* and *vincas* because they leave the microtubules arrays intact but merely attenuate microtubule dynamics just enough to activate mitotic checkpoints (Ye et al., 1998). Besides, unlike currently available microtubule drugs that either overpolymerize and bundle microtubules (*taxanes*) or depolymerize them (*vincas*), noscapinoids do not alter the monomer/polymer ratio of tubulin (Ye et al., 1998; Zhou et al., 2003) and thus they do not cause any hemo and neuronal toxicity based upon their unique mechanism of action. In pursuit of increasing its anticancer activity we have strategically designed a series of derivatives by modification of the scaffold structure.

CONTACT Pradeep Kumar Naik pknaik1973@gmail.com Centre of Excellence in Natural Products and Therapeutics, Department of Biotechnology and Bioinformatics, Sambalpur University, Jyoti Vihar, Burla, Sambalpur, Odisha 768 019, India

Supplemental data for this article can be accessed online at https://doi.org/10.1080/07391102.2020.1785945.

We have shown that these derivatives bind to tubulin with a higher affinity and do not alter the monomer/polymer ratio of tubulin In addition; these derivatives inhibit cellular proliferation and cause G2/M arrest in various human cancer cells followed by apoptotic cell death (Naik et al., 2011; Santoshi et al., 2011; Naik et al., 2012; Manchukonda et al., 2013; Manchukonda et al., 2014; Santoshi et al., 2015; Mahaddalkar et al., 2017). Noscapine and its derivatives were predicted to binds to α- and β- tubulin heterodimer interface near the colchicine site but not interfere with colchicine binding through use of computational docking techniques and molecular dynamic methods (Naik et al., 2011). This finding was supported by competitive binding experiments that indicated that noscapine was not competitive with colchicine (Naik et al., 2011). While several synthesized derivatives of noscapine showed promising *in vitro* activities against tumor cell lines, they were unable to achieve a complete elimination of the disease despite increased dosages.

Over the course of this decade, it is becoming well appreciated that more of a toxic drug at its maximum tolerated dose (MTD) is not necessarily better; and there is an opportunity to reduce its dose levels by using combination regimens of drugs that display synergistic interactions (Jordan & Wilson, 2004). In this context, the potential of combinatorial anti-microtubule therapy is an untapped source of chemotherapeutic wealth as the presence of diverse drug binding sites on tubulin suggest that rational combination of two or more drugs of this class might be able to enhance the anticancer efficacy and reduce toxic side effects, thereby, improving the therapeutic index. Previously it was demonstrated that the combination of docetaxel and other agents enhanced the anticancer activities of lung cancer (Hida et al., 2000; Hida et al., 2002; Nawrocki et al., 2004; Sweeney et al., 2005; Shaik et al., 2006) as well as breast cancer (Chougule et al., 2011). In the current study, we embark upon a approach to rationally designed a novel derivative of noscapine and evaluate its additive effect with the clinically approved anticancer agent, docetaxel, to enhance the anticancer activity.

Material and methods

Molecular modelling

Protein preparation

The co-crystallized structure of the colchicine-tubulin complex (PDB ID: 1SA0, resolution 3.58 Å) was used as a receptor protein. The errors in the PDB file were removed as per the procedure reported earlier (Santoshi & Naik, 2014). Further, refinement of the structure was achieved by energy minimization using Macromodel (Schrodinger package) and followed by molecular dynamic simulation of 100 ns using GROMACS 5.1.5 with similar parameters set up as reported earlier (Santoshi & Naik, 2014). A sum of 5000 frames was produced in the MD trajectories with a time step of 20 ps, from which the last 2000 frames were used to generate the average tubulin structure.

Rational design of novel derivative of noscapine

The lead molecule, noscapine is cytotoxic in a variety of different cancer cell lines (NCI 60 cell lines panel), although the IC_{50} value remain in the high micro-molar range (Naik et al., 2011). To enhance its anticancer activity further, efforts have been focused on rational designing and synthesis of new generation of noscapine derivatives. Noscapine docks onto $\beta-$tubulin near the interface between its dimerization partner, $\alpha-$tubulin (Checchi et al., 2003). This is supported by the earlier finding of 1:1 stoichiometry of tubulin binding (Ye et al., 1998). A closer look at the binding site revealed side chains around the putative binding pocket and the presence of an empty space around position 9 of noscapine. Inspired by the *in silico* findings, we have rationally coupled a bulky 4-vinyl phenyl functional group at the C-9 position of the noscapine scaffold in quest of developing a more potent derivative of noscapine (Figure 1).

Ligand preparation

The molecular structure of VPN and DOX was constructed using molecular builder of maestro (Schrodinger package). The built structures were energy minimized using Macromodel (Schrodinger package) and OPLS 2005 force field. For energy minimization, PRCG algorithm was used with 1000 steps and energy gradient of 0.001. Each ligand was assigned appropriate bond order using Ligprep. Further, the geometric optimization of the ligands was performed based on hybrid density functional theory with Becke's three-parameter exchange potential and the Lee-Yang-Parr correlation functional (B3LYP) (Lee et al., 1988; Becke, 1993) with basis set 3-21 G* (Binkley et al., 1980; Gordon et al., 1982; Pietro et al., 1982) using Jaguar (Schrödinger, LLC).

Molecular docking

Both VPN and DOX were docked onto αβ-tubulin heterodimer using "Extra Precision" (XP) algorithm of Glide docking (Schrödinger package) (Friesner et al., 2004; Halgren et al., 2004) in two cycles. The binding site of VPN is at the interface between α- and β- tubulin (noscapinoids binding site) (Naik et al., 2011), whereas the binding site of DOX is biased towards β-tubulin (taxol binding site) (Snyder et al., 2001). In the first cycle both DOX and VPN were docked onto their respective binding sites using Glide XP docking to calculate their individual binding affinity. In the second cycle, the VPN was docked onto the co-complex of DOX-tubulin and the DOX was docked onto the co-complex of VPN-tubulin. The binding sites were defined using a concentric grid box at the centroid of the binding site using the Glide grid-receptor generation program. An outer grid box of 12 Å x 12 Å x 12 Å was defined to confine the mass centre of the docked ligand. Besides, an enclosing grid box of 12 Å x 12 Å x 12 Å was defined which occupied all the atoms of the docked poses. The scale factor of 0.4 for van der Waals radii was applied to atoms of protein with absolute partial charges less than or equal to 0.25. The algorithm generated 10000 poses, out of which only 1000 poses were used for the minimization (conjugate gradients) and the final 30 structures

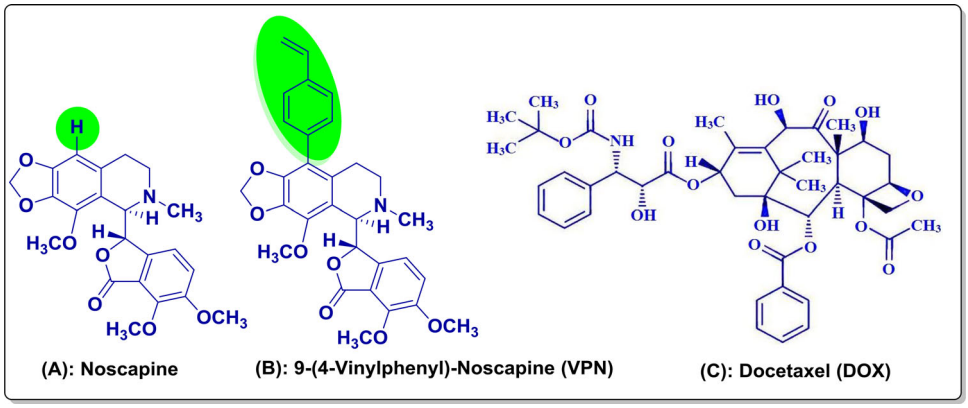

Figure 1. The molecular structures of (A) Noscapine (B) rationally designed derivative, 9-(4-vinylphenyl)-Noscapine (VPN) and (C) a clinical tubulin binding anti-cancer agent, Docetaxel (DOX) used in the study.

having the lowest energy conformations were evaluated for the favorable Glide docking score. A single best conformation for VPN and DOX was considered based on minimum docking score for MD simulation.

Molecular dynamics simulations

Co-complex of tubulin with both the ligands, VPN and DOX (Tub + VPN + DOX) was obtained from co-docking of DOX and VPN on Tubulin dimer (complex_1). GTP, GDP and magnesium ions were retained in the complex. Similarly, co-complex of tubulin-VPN (Complex_2) and Tubulin_DOX (Complex_3) were obtained by removing atoms of DOX and VPN from complex_1 respectively. Complex 4 with Tubulin only, without DOX and VPN, was also obtained. All simulations were performed using Amber 16 simulation suite (Case et al., 2016). The parameters for all 4 ligands such as DOX, VPN, GTP and GDP were estimated using Antechamber program of Amber 16 suite (Wang et al., 2006). All atomic point charges were calculated using AM1-BCC charge model (Jakalian et al., 2002). Topologies and internal coordinates for all complexes were generated using tleap program in Amber16. Missing Hydrogens were added and parameters were assigned to Protein and ligands using FF14SB and GAFF force-fields respectively (Maier et al., 2015). Each molecular system was neutralized by adding counter-ions and was subsequently solvated using TIP3P water model in a truncated octahedron with the distance of 12 Å between the atoms of protein and wall of the box (Jorgensen et al., 1983).

Once the topologies and internal co-ordinates for all complexes were obtained, three rounds of minimization were performed on each complex to relax the system and amend the bad contacts. Position restraints of 10 kcal/Å^2 and 2 kcal/Å^2 were imposed on the protein system for the first and the second rounds respectively, to relax the water molecules around protein. No restraints were imposed in the third round. After removal of bad contacts through minimization, all four molecular systems were equilibrated at 300 K and 1 atm for 500 ps. The equilibrated systems were then run for 100 ns each with time step of 2 fm. Throughout simulations the cut-off for non-bonded interaction was 10 Å, electrostatics was calculated using Particle Mesh Ewald (PME) and bonds were constrained using shake algorithm (Ryckaert et al., 1977; Darden et al., 1993; Essmann et al., 1995). Langevin thermostat was used to regulate the temperature of simulations. Co-ordinates were written every 20 ps to write 5000 frames for each molecular system. CPPTAJ implemented in Ambertools was used to analyze trajectories for Root Mean square deviation analyses (PTRAJ and CPPTRAJ, 2013).

Predictive binding affinity

Binding affinity of VPN and DOX was calculated when both ligands were bound to tubulin (complex 1). Binding affinity of VPN and DOX was also calculated when they were bound to tubulin separately in complex_2 and complex_3 respectively (Suri et al., 2015). Free energy of binding (ΔG_{bind}) was calculated as the ensemble average of the binding free energy of a total of 1000 snapshots, extracted every 20 ps from the last 20 ns of the MD simulation trajectory using MM-PBSA and MM-GBSA methods (Kollman et al., 2000; Massova & Kollman, 2000). as explained below:

$$\Delta G_{bind} = \Delta G_{complex} - \left[\Delta G_{Rec} + \Delta G_{lig}\right]$$
$$G = E_{gas} + G_{sol} - TS.$$
$$E_{gas} = E_{int} + E_{ele} + E_{vdw}$$
$$G_{sol} = G_{PB(GB)} + G_{sol-np}$$
$$G_{sol-np} = \gamma SAS$$

Where, G is Gibbs free energy, E_{gas} is the gas phase energy calculated as the sum of internal energy (E_{int}), energy generated as a result of the electrostatic interaction (E_{ele}) and the van der Waals interaction (E_{vdw}). G_{sol} is the solvation free energy calculated as the sum of polar ($G_{PB(GB)}$) and nonpolar contributions (G_{sol-np}). Polar interaction contribution ($G_{PB(GB)}$) was calculated as the summation of electrostatic contribution (E_{ele}) and polar solvation contribution ($G_{PB(GB)}$). The nonpolar solvation contribution (G_{sol-np}) is approximated as linearly dependent on the solvent accessible surface area (SAS) and γ is the surface tension constant that was set to 0.0072 kcal mol^{-1} Å^{-2} (Massova & Kollman, 2000).

Per residue energy decomposition

The contribution of each amino acid residue of tubulin was calculated to identify those residues which showed strong interaction with ligands (Suri et al., 2014). These calculations

were performed using MM-GBSA method implemented in Amber 16 over 1000 frames obtained every 20 ps from last 20 ns trajectory.

Chemistry

General

All the reactions were monitored by TLC (Precoated silica plates and visualizing under UVlight). Reagents and all solvents were analytically pure and were used without further purification. Air-sensitive reagents were transferred by syringe or double-ended needle. Evaporation of solvents was performed at reduced pressure by using heidolph rotary evaporator.^{1}H and ^{13}C NMR spectra of samples in $CDCl_3$were recorded on AVANCE-300 MHz, 400 MHz, 500 MHz spectrometer. Chemical shift reported are relative to an internal standard TMS ($\delta = 0.0$). Spin multiplicities are described as s (singlet), brs (broad singlet), d (doublet), t (triplet), q (quartet), or m (multiplet). Coupling constants are reported in hertz (Hz). Mass spectra were recorded in ESI conditions at 70 eV on LC-MSD (Agilent technologies) spectrometers. All high-resolution spectra were recorded on QSTAR XL hybrid MS/MS system (Applied Bio systems/MDS sciex, foster city, USA), equipped with an ESI source (IICT, Hyderabad). Column chromatography was performed on silica gel (60-120 mesh) supplied by Acme Chemical Co., India. TLC was performed on Merck 60 F-254 silica gel plates. Commercially available anhydrous solvents Dichloromethane, methanol, acetone and Ethylacetate were used as such without further purification. Natural α-noscapine was purchased from Sigma-Aldrich.

(S)-3-((R)-9-bromo-4-methoxy-6-methyl-5,6,7,8-tetrahydro-[1,3]dioxolo[4,5-g] isoquinolin-5-yl)-6,7-dimethoxyisobenzofuran-1(3H)-one (9-Br-nos)

To a suspension of natural α- noscapine (4.0 g, 9.7 mmol) was reacted with 48% aqueous HBr solution (15 mL) and saturated bromine water (~50 mL) following the procedure developed in our lab. The crude residue was purified over silica gel column chromatography eluted with 3:7 Ethyl acetate: Hexane (3:7) to give pure 9-bromonoscapine **2** (4.3 g, 90%) as white solid. mp 170 °C; $[\alpha]_D^{25}$=-106.8 ($c = 1$, Dichloromethane); ^{1}H NMR (300 MHz, $CDCl_3$) δ 6.96 (d, $J = 8.309$ Hz, 1H) , 6.26 (d, $J = 8.309$ Hz, 1H) , 6.023 (s,2H), 5.392 (d, $J = 4.721$ Hz, 1H), 4.270 (d, $J = 4.721$, 1H) , 4.077 (s, 3H), 3.999 (s, 3H) , 3.872 (s, 3H) , 2.831-2.746 (m, 1H), 2.670-2.579 (m, 1H) , 2.516(s, 3H), 2.496-2.422 (m, 1H), 2.024-1.913 (m, 1H). ^{13}C NMR (75 MHz, $CDCl_3$) δ 167.95, 152.24, 147.67, 146.47, 141.17, 139.90, 134.10, 130.26, 119.57, 118.90, 118.25, 117.45, 101.01, 95.50, 81.23, 62.24, 60.86, 59.37, 56.72, 48.34, 45.13, 25.85. MS (ESI) *m/z* 492 $[M + H]^+$; HR-MS (ESI) Calcd for $C_{22}H_{22}NO_7Br$ $[M + H]^+$:492.0657, found: 492.0636. The ^{1}H-NMR, ^{13}C-NMR and mass spectra (ESI and HR-MS) of the intermediate compound, 9-Br-noscapine are included as supporting material (S1 to S5).

(*S*) − 6,7-Dimethoxy-3- (*R*) − 4 - methoxy-6-methyl − 9 - (4-vinylphenyl) − 5,6,7,8 - tetrahydro-[1,3] dioxolo [4,5-*g*] isoquinolin-5-yl) isobenzofuran-1(3*H*) - zone (**9-VPN**): To a solution of 9-bromonoscapine (2.0 g, 4.1 mmol) in ethanol/toluene (1:1, v/v, 100 mL), $Pd(PPh_3)_4$ (0.59 g, 0.49 mmol), $NaHCO_3$ (8.2 mmol) and 4-vinylphenyl boronic acid (1.25 g, 8.2 mmol) were added sequentially, and the contents were stirred for 48 h at 120 °C. After the starting material was completely consumed in the reaction (judged by TLC), reaction mixture was cooled to room temperature, the solvents were evaporated under vacuum. The crude residue was extracted into dichloromethane (3 × 25 mL) and washed with brine solution. The organic layer was collected and passed through a Na_2SO_4 bed and later removed under reduced pressure. The crude residue was chromatographed over a triethylamine silica gel bed, using pet. ether/ethyl acetate (7:3) as eluents, to give pure compound as colourless solid. (1.32 g) Yield: 62%; m.p: 120-122 °C; $[\alpha]_D^{25}$ 120.22 ($c = 1$, dichloromethane); ^{1}H NMR (300 MHz, $CDCl_3$): δ 7.40 (d, $J = 8.24$ Hz, 2H), 7.17 (d, $J = 8.24$ Hz, 2H), 6.97 (d, $J = 8.16$ Hz, 1H), 6.74-6.66 (dd, $J = 10.81$ Hz, 17.51 Hz, 1H) 6.10 (s, 1H), 5.98 (s, 1H), 5.91 (s, 1H), 5.74 (d, $J = 17.51$ Hz, 1H), 5.48 (s, 1H), 5.25 (d, $J = 10.81$ Hz, 1H), 4.47 (s, 1H), 4.10 (s, 6H), 3.90 (s, 3H), 2.66-2.54 (m, 4H), 2.27-2.13 (m, 2H), 1.77-1.64 (m, 1H). ^{13}C NMR (75 MHz, $CDCl_3$): δ 157.9, 152.2, 147.7, 146.0, 143.6, 140.9, 139.6, 136.7, 133.7, 133.5, 130.7, 130.1, 126.0, 120.4, 117.8, 116.1, 114.2, 100.8, 81.9, 62.3, 61.1, 59.5, 56.9, 50.8, 46.6, 27.0, 23.2, 29.6. MS (ESI): m/z 538 $[M + Na]^+$; HRMS (ESI): Calcd for $C_{30}H_{29}NO_7$ $[M + Na]^+$; 538.1841; found: 538.1848. The ^{1}H-NMR, ^{13}C-NMR and mass spectra (ESI and HR-MS) of the final product, VPN are included as supporting material (S6 to S9).

Biology

Cell culture and reagents

The natural lead compound, noscapine and docetaxel were obtained from Sigma. All the chemical reagents and media used for cell culture were obtained from Mediatech, Cellgro. Human breast cancer cell line, MCF7 was obtained from the cell repository of the National Center for Cell Science Pune, Maharashtra, India. Stock solution (100 mM) of the newly synthesised noscapine derivative, VPN was prepared with dimethyl sulfoxide (DMSO) and stored at 4 °C until use. The cells were allowed to grow at a temperature of 37 °C in a 5% CO_2 and 95% humidity in Dulbecco's modified Eagle medium (DMEM, Pan Biotech), supplemented with 10% fetal bovine serum (FBS) and antibiotics.

In vitro cell proliferation assay

Inhibition of cell proliferation of MCF7 was assessed by 3-(4, 5-dimethylthiazol-2-yl)-2,5, ditetrazolium bromide (MTT) assay. Briefly, MCF 7 cells (3×10^3) were seeded into 96 well plates. After post attachment of 48 h, the cells were treated with different concentrations of VPN alone (10, 25, 50, 100 μM), DOX alone (0.001, 0.01, 0.1,1,10 μM) and in combination of VPN and DOX (10 μM VPN + 0.001 μM DOX, 15 μM VPN + 0.01 μM DOX, 20 μM VPN + 0.05 μM DOX, 25 μM VPN + 0.1 μM DOX, 30 μM VPN + 0.5 μM DOX). Cells were incubated for 48 h and 72 h. After the stipulated time the cells were incubated with 10 μl of MTT (5 mg/ml) for 4.0 h, at

37° C and the absorbance was measured in plate reader (Varioskan, Thermo Scientific) at 570 nm. The value of IC_{50} (the concentration of the drugs required to prevent cell proliferation by 50%) of VPN alone, DOX alone and in combination regimen of VPN and DOX was determined. The experiments were repeated in triplicates.

Cell cycle analysis

MCF7 (1×10^5) cells were seeded into a 6-well culture plate. After 24 h the cells were treated with VPN alone (20 μm), DOX alone (0.5 μm) or in combination regimen of VPN and DOX (25 μm VPN + 0.05 μm DOX). Cells were harvested after 24 h of treatment using trypsin-EDTA, washed properly with phosphate buffered saline (PBS) and fixed in 70% ethanol for 30 min. After fixation, the cells were stained with staining solution that included RNase (5 μg/ml), propidium iodide (5 μg/ml) and Triton X (0.1%). In Flow cytometer (FACS Calibur), the cells were analysed to monitor the inhibition in cell cycle progression. The experiment was performed in triplicates.

Apoptosis assay

MCF7 cells (5×10^4) were seeded in 35 mm plates. After 24 h, cells were treated with VPN alone (20 μm), DOX alone (0.5 μm) or in combination regimen of VPN and DOX (25 μm VPN + 0.05 μm DOX) at a temperature of 37 °C and 5% CO_2. Cells were sampled and analyzed using flow cytometry after 24 h of treatment. Briefly, the cells were stained with propidium iodide (PI) and Annexin-V-Alexa Fluor 488 (BD Pharmingen, San Diego, CA, USA) according to the manufacturer's protocol. Percentage of apoptotic cells were assessed using BD FACS Calibur (San Jose, CA, USA).

DAPI staining

The apoptotic cells in presence of VPN (20 μm), DOX (0.5 μm) and in combination regimen (25 μm VPN + 0.05 μm DOX) were visualized by staining with DAPI under fluorescence microscopy. In brief, MCF7 cells (3×10^3 cells) were grown on poly-l-lysine coated coverslips in 6-well plates and treated with single as well as in combination regimen for 48 h. The cells were then washed twice with ice-cold PBS. The coverslips were fixed with 70% ethanol and stained using DAPI, followed by imaging using BX60 fluorescence microscope (Olympus, Tokyo, Japan). Apoptotic cells were identified as changes in cellular morphology (e.g. nuclear condensation, membrane blebs formation, and apoptotic bodies).

Tubulin purification

Microtubules were isolated and purified from the goat brain through alternative cycles of GTP-dependent polymerization and depolymerisation in PEM buffer (50 mM pipes, 3 mM MgSO4, 1 mM EGTA, pH 6.8) (Hamel & Lin, 1981; Panda et al., 2000). The purified microtubules were preserved at −80 °C. The purified tubulin was estimated using the Bradford method as well as by SDS PAGE (Bradford, 1976).

Tryptophan quenching assay

Tubulin (2 μM) was incubated in a water bath with VPN at a concentration of 20 μM, DOX at a concentration of 0.5 μM and in combination regimen (DOX 0.05 μM + VPN 25 μM) in PEM buffer (50 mM pipes, 3 mM MgSO4, 1 mM EGTA, PH 6.8) for 45 min at 35 °C. The samples were excited at 295 nm and emission was measured at 310-400 nm. For the spectrofluorometric titrations a FlouroMax® 4 spectrofluorometer (Horiba Scientifc, Edison, NJ) assisted by Fluor Essence 3.5 software was used. The experiments were repeated twice.

ANS (8-Anilino-1-naphthalene sulfonic acid)-binding assay

ANS binding assay was performed to verify the structural integrity of the tubulin in presence of VPN and DOX in single as well as in combination regimen. Tubulin (2 μM) was incubated with VPN (20 μM and 50 μM), DOX (0.5 μM) and in combination regimen (DOX 0.05 μM + VPN 25 μM) at 35 °C for 30 min in PEM buffer. ANS (50 μM) was added and the samples were incubated in dark at 25 °C for 15 min. The samples were excited at 350 nm and the emission was measured at 410–470 nm using a Flourolog 3 spectrofluorometer (Horiba Scientific, Edition, NJ) assisted by fluorescence 3.5 software. The assays were repeated two times.

Results and discussion

Molecular modelling

Both noscapinoid and docetaxel were reported to bind to tubulin at a different site. Noscapinoids bind at the interface of α- and β- tubulin (Naik et al., 2011), whereas the binding of docetaxel was biased to β-tubulin (Snyder et al., 2001). Since both the ligands bind to tubulin, we are interested to determine the binding affinity of both VPN and DOX when both the ligands are docked at their respective binding site onto tubulin. We have performed two cycles of molecule docking with tubulin. In the first cycle DOX was docked onto its binding site and similarly VPN was docked onto noscapinoid binding site using Glide XP docking to calculate their binding affinity, individually. Both the ligands, VPN and DOX docked well into their binding site with a docking score of −4.82 kcal/mol and −6.67 kcal/mol respectively (Table 1). The DOX-tubulin complex was taken in the second cycle and the VPN was docked onto the noscapinoid binding site. Presence of DOX on its binding site interfered with the binding of VPN with a reduced docking score of −3.232 kcal/mol. It may be because of the alteration of the secondary conformation of tubulin due to binding of DOX.

MD simulation of the complex

We determine the binding mode of both VPN and DOX independently with tubulin (Tub-VPN and Tub-DOX complexes) as well as in the presence of both of them in their respective binding site onto tubulin (Tub-DOX + VPN) by molecule dynamic simulation of 100 ns to obtain a trajectory of 5,000 frames, each frame recorded every 20 ps. Root mean square deviations (RMSD) of Cα-atoms during the entire duration of

Table 1. Molecular docking results (Glide XP_{score}) and the relevent energy parameters of VPN and DOX in single as well as in combination with tubulin.

Ligands	Glide XP_{score} (kcal/mol)	Glide E_{vdw} (kcal/mol)	Glide E_{coul} (kcal/mol)	Glide energy (kcal/mol)
VPN	−4.82	−39.86	−8.16	−48.02
DOX	−6.67	−41.63	−8.46	−50.09
VPN-DOX	−3.23	−32.83	−9.27	−42.10

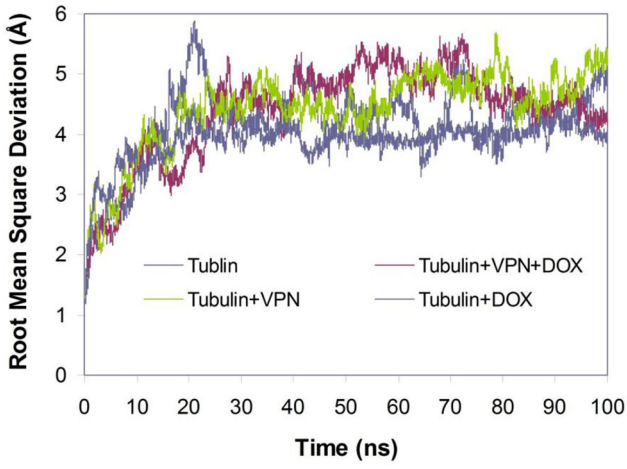

Figure 2. Root mean square deviations (RMSD) of Cα carbon atoms of tubulin only and in complex with VPN (Tubulin + VPN), with docetaxel (Tubulin + DOX) and with both docetaxel and VPN (Tubulin + DOX + VPN) during 100 ns of MD simulation. The relative fluctuation in the RMSD of the Cα atoms is very small after ~ 20 ns of the simulation. The time step of 20ps was used during the simulation that generated 5,000 frames which were used to generate the average structure.

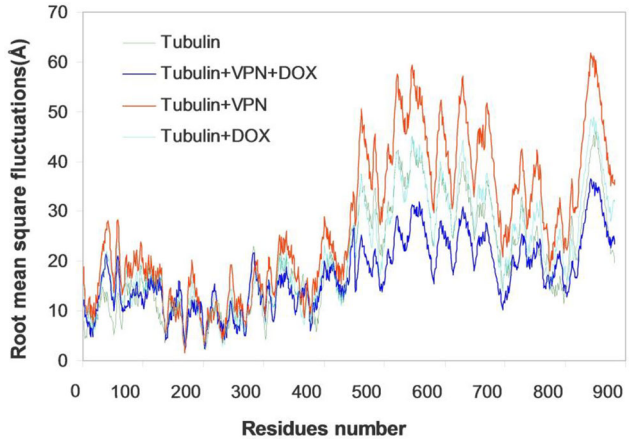

Figure 3. Root mean square fluctuation (RMSF) of the residues of tubulin of the docked ligands in the bound form and in the unbound form of tubulin heterodimer. Different levels of flexibility of these residues were noticed in the bound form of tubulin with VPN and DOX in single as well as in combination. Most of the residues showed flexibilities >5 Å in case of tubulin bound with VPN and DOX as compared to the free tubulin heterodimer, indicating that these residues seem to be more flexible as a result of binding.

simulation were calculated for all the frames to monitor the stability of the system (Figure 2).

All the systems got stabilized after 20 ns of simulation, since the relative fluctuation in the RMSD of Cα carbon atoms (Cα-rmsd) was very small after equilibration. The overall RMSD ranges from 0 to 2.582 Å. Furthermore, root mean square fluctuations (RMSF) of Cα-atoms were also calculated for all the systems to find any changes in the residue flexibilities. The RMSF values were plotted against residue numbers based on the 100 ns trajectory (Figure 3). The residues with higher RMSF tend to show more flexibility. Both VPN and DOX were well accommodated inside the binding cavity. The VPN docked well at the interface of α- and β- tubulin, whereas the binding of DOX is biased more towards β-tubulin (Figure 4a and b). Their binding mode with the tubulin was represented in two steps: (a) receptor residues that have strong interactions with the ligand, such as a favourable hydrogen-bonding interactions, and (b) receptor residues that are close to the ligand, but whose interactions with the ligand are weak or diffuse, such as hydrophobic interaction.

The differential mode of interactions of compounds VPN and DOX with the residues of tubulin are represented in the Ligplot. The differences in amino acids for binding of VPN with tubulin independently and in combination with DOX (Figure 4c and d) were mainly because of the change in conformation of tubulin due to binding of DOX. Similarly, the differences in amino acids for binding of DOX with tubulin, independently and in combination (Figure 4e and f) were due to change in the conformation of tubulin upon binding of VPN. As seen in the figure several hydrogen bonds and hydrophobic interactions are involved in their binding.

The amino acids of the binding site involved in the binding of VPN are Glu 336(D),Val 351(D), Leu 333(D),Pro 175(A), Glu 207(A), Arg 340(A), Asn 337(D), Lys 394(A) (Figure 4c), and the DOX are Val 23(D), Ala 233(D), His 229(D), Asp 226(D), Leu 219(D), Leu 371(D), Arg 278(D), Arg 369(D), Gly 370(D) (Figure 4d). The two hydrogen bonds contributed to the interactions of VPN with the binding pocket of tubulin. The oxygen atom (O_2) of the isoquinoline ring is hydrogen-bonded with the ND2 of the side chain of Leu D 286 with a distance of 3.04 Å. The carbonyl oxygen of isobenzofuran ring is hydrogen-bonded with the side chain of Arg D 278 with the distance of 3.05Å'. Similarly, binding of DOX involves two hydrogen bonds; the amino acids Lys 372, Leu 371, Gly 370, Leu 286 and Gln 281 contributed to hydrophobic interactions with the ligands. The isoquinoline ring is hydrogen-bonded with ND2 of the side chain of Asn D 337 with a distance of 3.21 Å and the isobenzofuran ring is hydrogen-bonded with the side chain of Lys A 394 with the distance of 2.90 Å. In contrast, there is significant difference in the amino acids involved in the interaction of VPN as well as DOX in the co-complex of tubulin with both the ligands together (Figure 4e and f) This clearly explains the changes in the binding mode of VPN and DOX when both the ligands are docked together with the tubulin so there is a chance of combination effect.

Calculated binding affinities of VPN and DOX

The binding free energy and its respective components of both VPN and DOX with tubulin were calculated independently as well as in combination and presented in Table 2. We have considered last 250 frames from the last 5 ns of trajectory

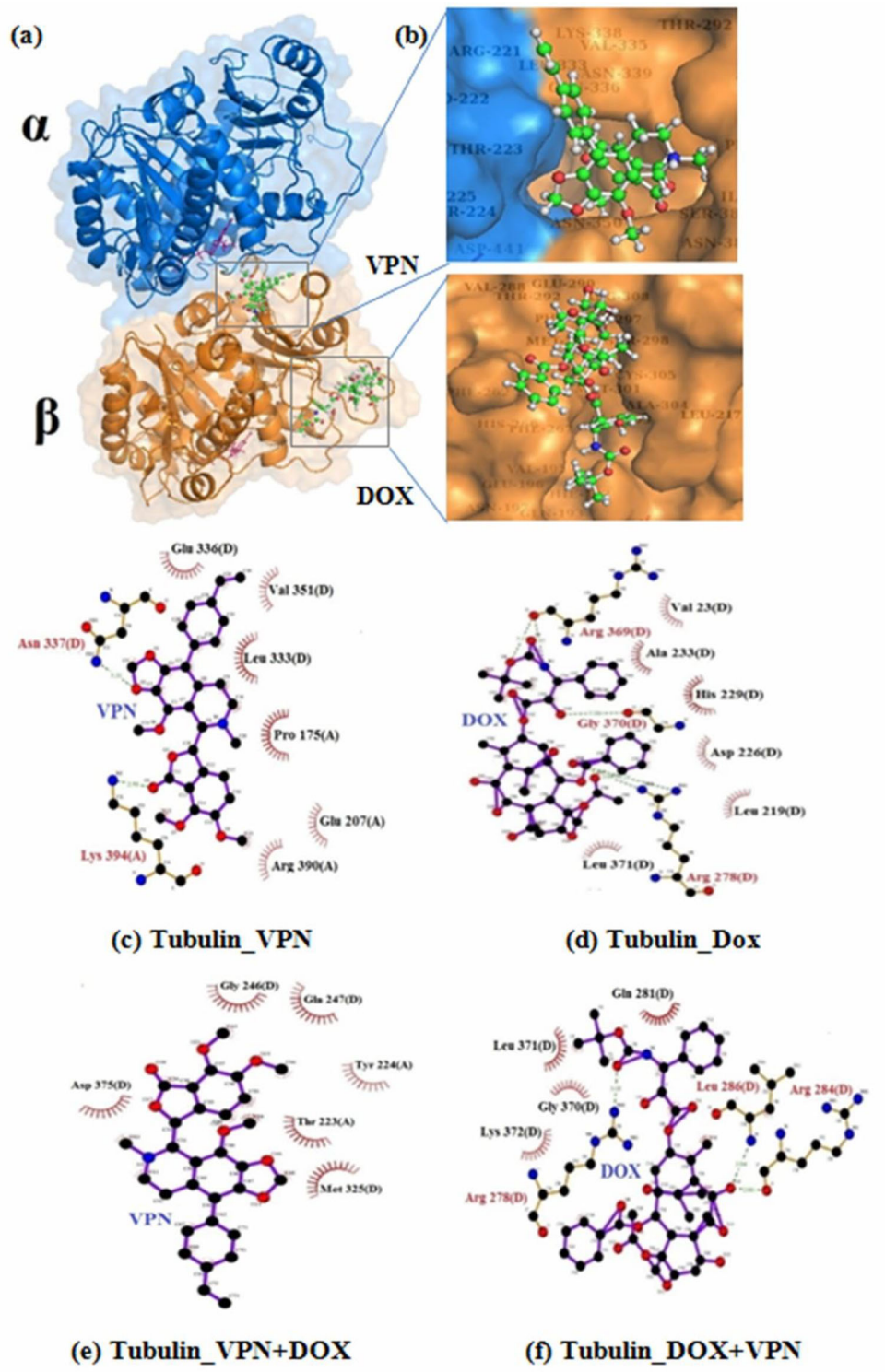

Figure 4. (a) Both VPN and DOX are well accomodated inside their respective binding site of tubulin. (b) Snapshot of both the ligands are obtained from the MD simulation. The binding site is represented as macromodel surface according to α- and β- tubulin (α-tubulin is represented in blue colour and β-tubulin is represented in brown colour). The ligplot analysis showing the interaction of binding site amino acids with the (c) VPN, (d) DOX, (e) VPN when it is docked into the co-complex of tubulin and DOX, and (f) DOX when it is docked into the co-complex of tubulin and VPN. The binding site residues involved in the interaction of VPN and DOX are slightly different in single as well as combine docking. The hydrogen bonds formed (if any) are represented as dotted lines.

to calculate the ensemble average of the free energy of binding using both MM-GBSA and MM-PBSA methods. For all complexes, the binding energy was decomposed into its various energy components (the electrostatic, van der Waals and solvation). Both van der Waals (ΔE_{VDW}) and the electrostatic component (ΔE_{ELE}) were observed to make very significant contributions to the free energy of binding. However, the net polar contribution ($\Delta G_{(ele,PB/GB)} = \Delta E_{ele} + \Delta G_{(PB/GB)}$) was rendered unfavourable due to very large penalty imposed by the desolvation component ($\Delta G_{PB/GB}$) while the net nonpolar component (ΔE_{vdw}) and ($\Delta G_{sol\text{-}np}$) were observed to have made highly favourable contribution to the binding free energy.

The results obtained from both the methods suggested very robust interactions of both VPN and DOX independently

as well as in combination. The predicted binding free energies (ΔG_{bind}) based on MM-GBSA method for VPN and DOX independently are −24.12 kcal/mol and −20.07 kcal/mol and in combination of both are −19.99 kcal/mol and −24.17 kcal/mol respectively. In contrary the ΔG_{bind} based on MM-PBSA for VPN and DOX independently are estimated to be −24.04 kcal/mol and −18.65 kcal/mol and in combination of both are −21.41 kcal/mol and −22.70 kcal/mol. The differences in the calculation of ΔG_{bind} between both the methods derived from the difference in calculation of the contribution to the polar solvation energy, which is slightly higher in the MM-PBSA calculation compared to MM-GBSA. Very robust van der Waals (ΔE_{VDW}) interactions of VPN, to the magnitude of −33.51 kcal/mol to −30.34 kcal/mol were observed for the single and combination with DOX. Similarly, the ΔE_{VDW} interactions of DOX, to the magnitude of −34.04 kcal/mol to −35.39 kcal/mol were observed for the DOX in single as well as in combination with VPN. The net polar component ($\Delta G_{GB\text{-}polar}$) was observed to be unfavourable in the interaction of VPN and DOX with tubulin (Table 2). The unfavourable polar contributions were observed to have overcome the highly favourable non-polar components ($\Delta G_{sol\text{-}np}$) among both the dimers. Interactions of VPN and DOX with tubulin seem to be steered by nonpolar component. This can be explained by the tendency of the nonpolar residues to readily bury themselves in the hydrophobic pockets and displaced water.

Table 2. Calculated binding energy and its various componentes (kcal/mol) of VPN and DOX in single as well as in combination binding with tubulin. The values in bold represent the ΔGbind energy of molecules with tubulin based on MM-GBSA and MM-PBSA methods.

Energy component	Tub_VPN	Tub_Dox	Tub_DOX + VPN	Tub_VPN + DOX
ΔE_{VDW}	−33.51	−34.04	−30.34	−35.39
ΔE_{ELE}	−289.96	−11.21	−313.55	−20.00
ΔE_{GAS}	−323.46	−45.26	−343.88	−55.40
$\Delta G_{GB\text{-}Polar}$	303.25	29.70	327.49	35.98
$\Delta G_{SOL\text{-}NP}$	−3.92	−4.51	−3.60	−4.75
$\Delta G_{SOL\text{-}GB}$	299.33	25.19	323.90	31.23
$\Delta G_{bind\text{-}GBSA}$	**-24.12**	**-20.07**	**-19.99**	**-24.17**
ΔG_{PB}	303.16	30.92	325.94	36.8913
$\Delta G_{SOL\text{-}NP}$	−3.74	−4.31	−3.46	−4.1931
$\Delta G_{SOL\text{-}PB}$	299.42	26.61	322.48	32.6982
$\Delta G_{bind\text{-}PBSA}$	**-24.04**	**-18.65**	**-21.41**	**-22.7061**

Per residue energy decomposition

Energy contribution of each residue in the binding of VPN and DOX was calculated using the MM-GBSA method to investigate the details of protein-ligand interactions at the atomic level. The predictive binding energy ($\Delta G_{bind,GB}$) of VPN and DOX independently was decomposed into per residue basis and included in (Figure 5a). Per residue contribution of binding free energy is an efficient way to investigate the details of protein–ligand interactions at the atomic level. We have identified the residues that have the greatest impact, in terms of total energy (ΔG_{bind}) contribution, known as hotspot amino acids. For the binding of VPN, residue Met323 showed the largest contribution (< -1.0 kcal/mol), while five other binding site residues (Glu183, Gln245, Asp327, Ala352 and Val353) contributed energy > -1.0 kcal/mol (Figure 5a). Moreover, the hot spot amino acids make considerable electrostatic energy contribution towards the binding of VPN. The hotspot amino acids in the binding of VPN were slightly different in presence of DOX. For the binding of DOX, residues Ala283, Leu361, Lys362 and Met363, showed the largest contribution of < -1.0 kcal/mol, whereas four other amino acids Tyr281, Arg282, Ala283 and Leu284) contributed > -1.0 kcal/mol energy (Figure 5b). All these hot spot amino acids make considerable van der Waals energy contribution towards the binding of DOX. The hospot amino acids were found to be diffferent in the presence of VPN.

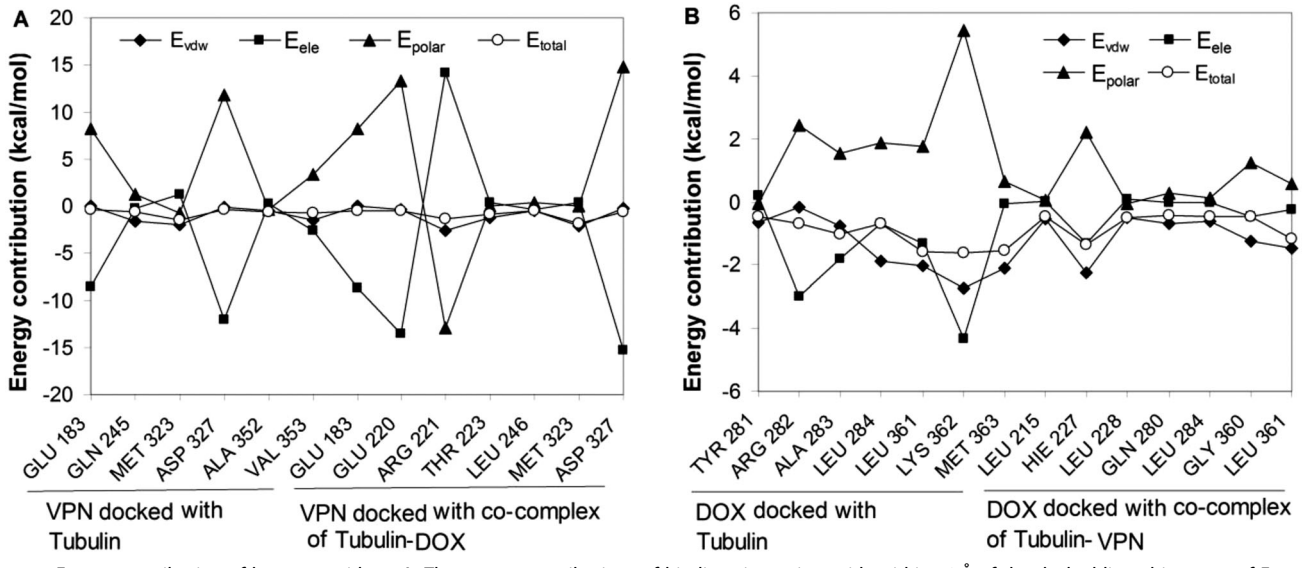

Figure 5. Energy contribution of hotspot residues. A. The energy contributions of binding site amino acids within 12 Å of the docked ligand in terms of E_{vdw}, E_{ele}, E_{polar} and E_{total} with VPN when it docked in single with the tubulin as well as in the co-complex of tubulin-DOX (A) and with DOX when it docked in single with the tubulin as well as in the co-complex of tubulin-VPN (B). For binding of VPN the hotspot amino acids make considerable electrostatic interaction energy, whereas for binding of DOX the hotspot amino acids make considerable van der Walls interaction energy. Further, for the binding of VPN and DOX with tubulin only and in co-complex with the ligands slightly different set of binding site amino acids are involved.

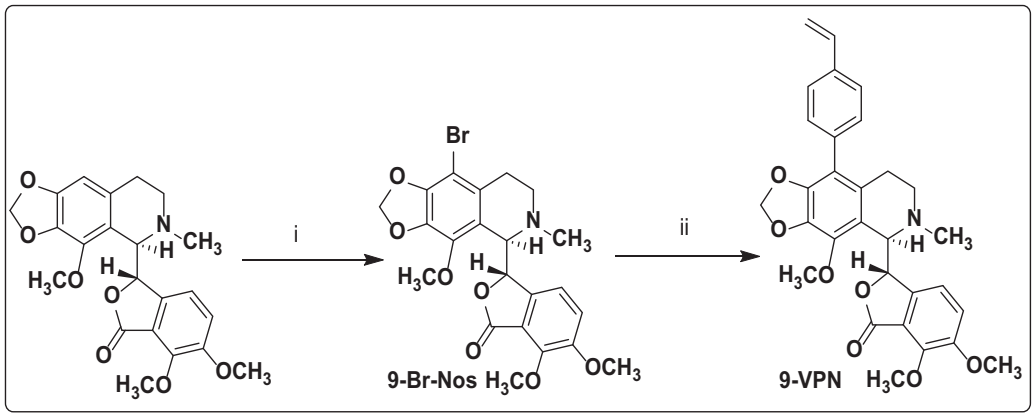

Scheme 1. Reaction Conditions. (i) 48% HBr, Br_2-water, RT, 2 h, 90% (ii) 4-Vinylphenyl boronic acid, Pd $(TPP)_4$, $NaHCO_3$, EtOH/Toluene, 120 °C, 48 h, 60%.

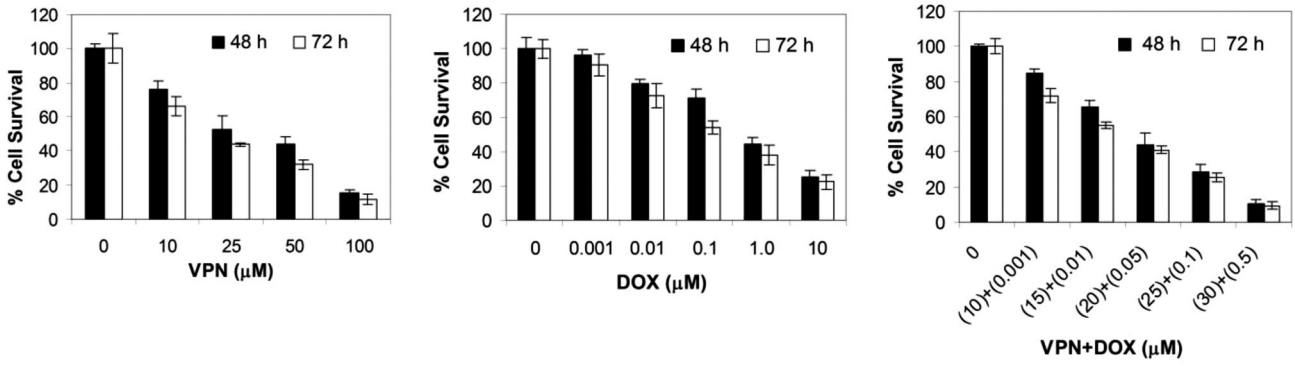

Figure 6. The inhibition of cellular proliferation of human breast cancer cell, MCF-7 with the treatment of VPN and DOX in single as well as in combination regimen at different concentration after 48 h and 72 h post-treatment. The IC_{50} value amounted to 30.17 μM and 19.92 μM, respectively for 48 h and 72 h with VPN. Similarly, the IC_{50} value amounted to 0.621 μM and 0.193 μM, respectively for 48 h and 72 h with DOX. In contrast, the approximately 50% inhibition of cellular inhibition was achieved in a combination regimen of VPN (20 μM) and DOX (0.05 μM) after 48 h and 72 h post-treatment.

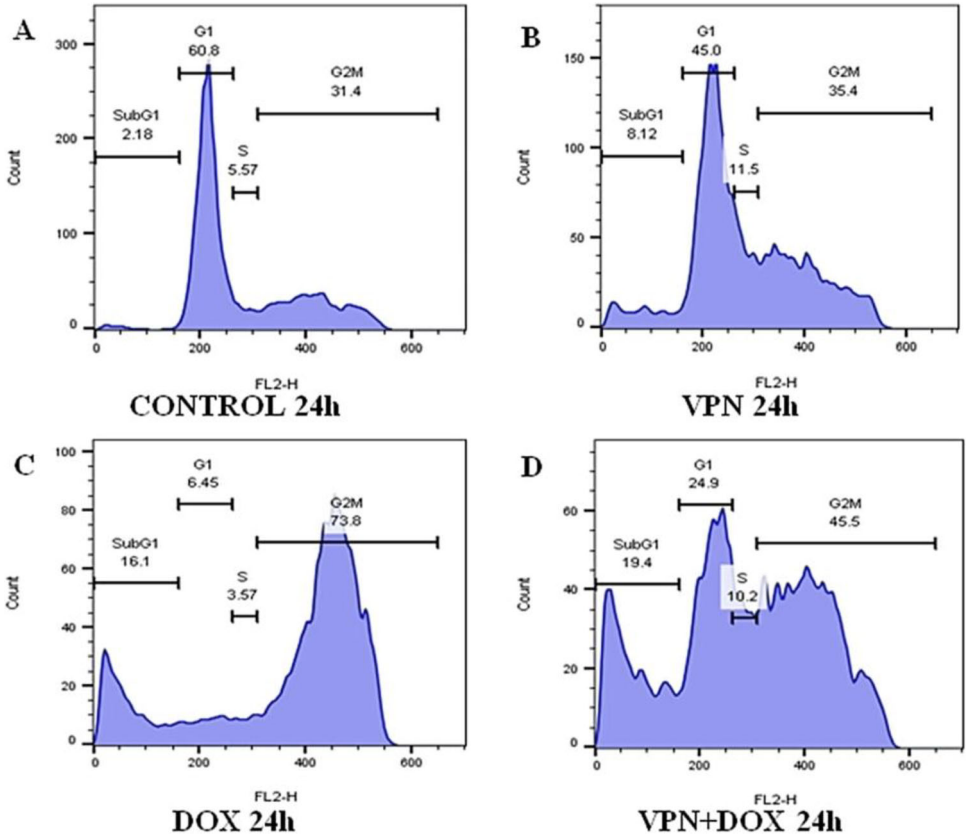

Figure 7. Panels (A) to (D) depicts cell cycle distribution of MCF-7 cells in a two-dimensional disposition as determined by flow cytometry at 24 h of treatment with 20 μM of VPN, 0.5 μM of DOX as single regimen and 25 μM of VPN + 0.05 μM of DOX in combination regimen. Results represent cell cycle progression at mitosis followed by the appearance of a characteristic hypodiploid (sub-G1) DNA peak is indicative of apoptosis.

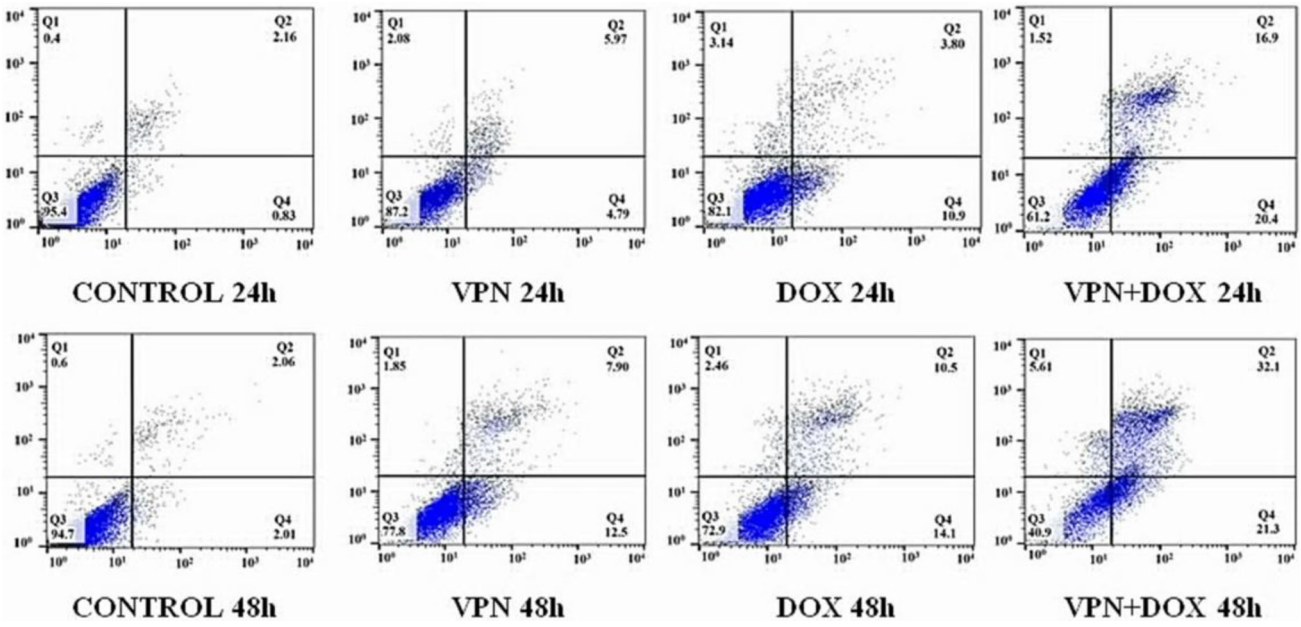

Figure 8. Induction of apoptosis caused by VPN (20 μM) and DOX (0.5 μM) alone and in their combination regimen (VPN, 25 μM + DOX, 0.05 μM) based on flow cytometric analysis. PE/Annexin V staining was used in combination with 7-Amino-Actinomycin (7-AAD) to distinguish among 4 subpopulations: cells negative for both 7-AAD and Annexin V staining were viable cells (in the lower left quadrant: Q3); 7-AAD-negative, Annexin V-positive cells were early apoptotic cells (in the lower right quadrant: Q4); 7-AAD-positive, Annexin V-positive cells were primarily late apoptotic/necrotic cells (in the upper right quadrant: Q2); and the 7-AAD-positive but annexin V-negative cells were necrotic cells (in the upper left quadrant: Q1).

Chemistry

It is always a challenge to synthesize the derivatives of noscapine because of their highly sensitive C-C bond between isoquinoline and isobenzofuranone ring components which are labile to strong acids and base. However, we have optimized the reaction conditions for the amalgamation of the VPN from 9-bromonoscapine as starting material without affecting the sensitive C-C bond (Scheme 1).

The starting material 9-bromo noscapine required was synthesized from natural α-noscapine in excellent yield (90%) using bromine water in 48% aqueous HBr by modifying the reaction conditions described in literature (Naik et al., 2011). 9-bromonoscapine reacted with 4-vinyl boronic acid, $Pd(TPP)_4$, $NaHCO_3$ in ethanol/toluene at 120 °C for 48 h to give VPN in 60% yield. Both 9-Br-Noscapine and VPN were fully characterised by ^1H, ^{13}C NMR and mass (ESI and HRMS), IR spectral data (supporting material S1-S9).

Biology

VPN inhibits proliferation of cancer cells

Inspired by the *in silico* prediction of binding affinity of VPN with tubulin dimer, we evaluated its efficacy in inhibiting proliferation of MCF7 cells in single and in combination regimen with DOX. The anti-proliferative activity for both VPN and DOX increases with the increasing concentration in single as well as in combination regimen (Figure 6). The IC_{50} value amounted to 30.17 μM and 19.92 μM, respectively for 48 h and 72 h with VPN. Similarly, the IC_{50} value amounted to 0.621 μM and 0.193 μM, respectively for 48 h and 72 h with DOX. Surprisingly, the inhibition of cellular proliferation was significantly achieved with the combination dose regimens of both VPN and DOX. The approximately 50% inhibition of cellular proliferation was found to be at VPN (20 μM) and DOX (0.05 μM). The dose dependent cytotoxicity of DOX has been reduced considerably with the combination dose regimen of VPN.

Cell cycle analysis

Inhibition in the progression of cell cycle of MCF7 with treatment of VPN (20 μM) and DOX (0.5 μM) in single regimen as well as in combination regimen (25 μM VPN + 0.05 μM DOX) was evaluated using flow cytometer. Both the compounds showed an increase in the sub-G1 cell populations compared to the control after 24 h of treatment in single and in combination regimen. The representative two-dimensional disposition of cell cycle profile is included in Figure 7. The sub-G1 population with treatment of VPN was increased to 8.12%, whereas with DOX it was increased to 16.1% and in combination it further increased to 19.4% in comparison to control. A cell must lose enough DNA to appear in the sub-G1 area. Therefore, both the compounds, VPN and DOX in single as well as in combination induce apoptosis to cancer cell. Maximum cells were arrested at the G2M transition phase.

Apoptosis assay

We approached to determine the induction of apoptotic cell death to breast cancer cell, MCF-7 by treatment of VPN and DOX in single as well as in combination regimen. Biochemically, the early apoptotic stage is characterized by the loss of lipid asymmetry between the two plasma membrane leaflets, resulting in an irregular externalization of phosphatidylserine (PS) from the inside leaflet to the outer leaflet, which can be measured fluorescently by annexin V

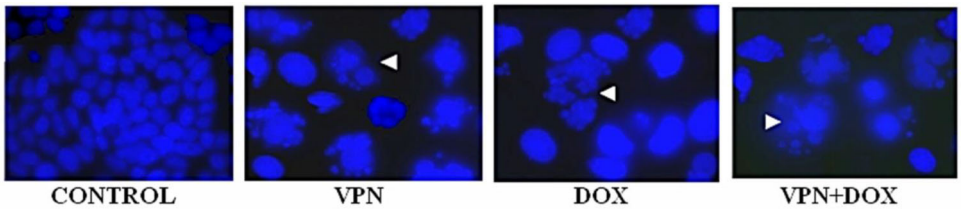

Figure 9. Morphologic indicators of apoptotic cell death include chromatin condensation along with nuclear envelope and plasma membrane blebbing followed by formation of small apoptotic bodies. Panels show morphological evaluation of nuclei stained with DAPI in the absence and presence of the VPN (20 μM) and DOX (0.5 μM) in single as well as in combination regimen (25 μM VPN + 0.05 μM DOX). Several typical features of apoptotic cells such as condensed chromosomes, numerous fragmented micronuclei, and apoptotic bodies are evident (indicated by white head arrows) upon 48 h of drug treatment. (Scale bar = 15 μm).

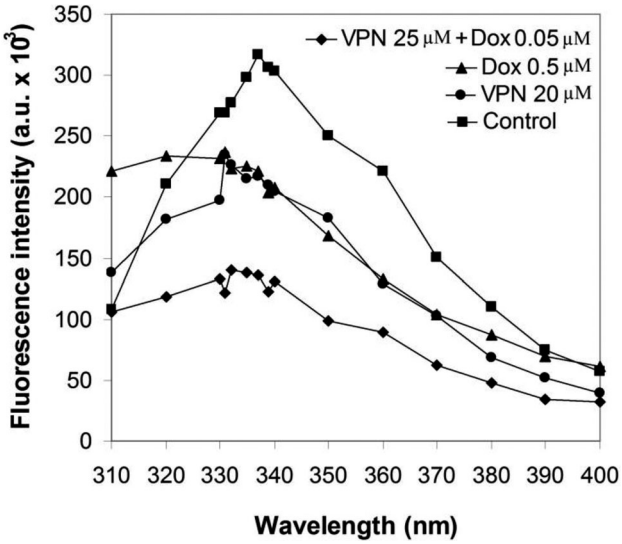

Figure 10. Decrease of fluorescence intensity of tubulin by VPN and DOX in single as well as in combination regimen. Tubulin (2.0 μM) was incubated with VPN (20 μM) and DOX (0.5 μM) alone as well as in combination regimen (25 μM of VPN + 0.05 μM of DOX) and the emission spectra were collected (310 nm – 400 nm). Both VPN and DOX in single as well as in combination regimen showed a concentration-dependent quenching of the intrinsic tubulin fluorescence emission intensity indicating the binding of both VPN and DOX to tubulin. The more reduction in tubulin fluorescence intensity in combination regimen of both VPN and DOX, compared to their single binding, revealed combination effect with the tubulin. The graph is a representative of three independent experiments.

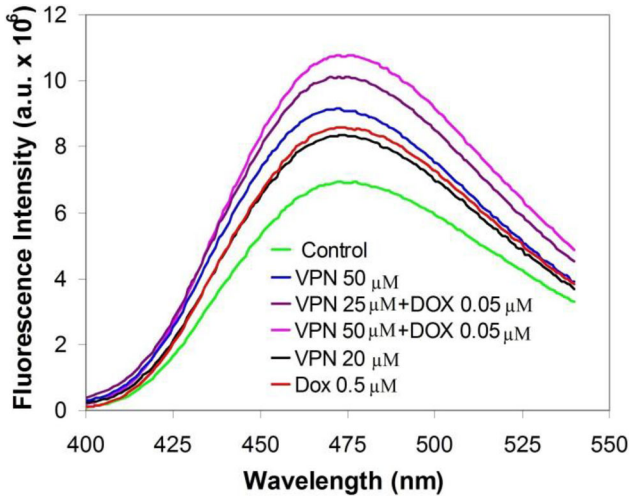

Figure 11. Enhancement of tubulin-ANS fluorescence by VPN and DOX in single as well as in combination regimen. Tubulin (2.0 μM) was incubated without (control) or with VPN (50 μM and 20 μM), DOX (0.5 μM) and in their combination regimen (VPN 25 μM + DOX 0.05 μM, VPN 50 μM + DOX 0.05 μM), followed by incubation with ANS (50 μM). The samples were excited at 380 nm and the emission spectra were collected (390 nm – 500 nm). Both VPN and DOX in single as well as in combination regimen showed a concentration-dependent increase in tubulin-ANS fluorescence indicating the binding of both VPN and DOX to tubulin. The increase is more in tubulin-ANS fluorescence in combination regimen of both VPN and DOX, compared to their single binding, revealed combination effect with the tubulin. The graph is a representative of three independent experiments.

binding. In contrast, a cell-impermeant DNA-binding fluorescent dye, propodium iodide can only enter the cells when it is at the stage of late apoptosis when membrane permeability is compromised. The apoptotic cells can be quantified to a large extent by FACS analysis. In FACS analysis, green Annexin V staining was used together with an impermeant red DNA binding dye, 7-Amino-Actinomycin (7-AAD), to quantitate the population of apoptotic, necroptotic and necrotic cells. Figure 8 depicts the density plots of 7-Amino-Actinomycin (7-AAD) versus PE conjugated Annexin V fluorescence obtained from untreated control and treated MCF7 cells. Cells negative for both 7-AAD and Annexin V staining were viable cells (in the lower left quadrant: Q3); 7-AAD-negative, Annexin V-positive cells were early apoptotic cells (in the lower right quadrant: Q4); 7-AAD-positive, Annexin V-positive cells were primarily late apoptotic/necrotic cells (in the upper right quadrant: Q2); and the 7-AAD-positive but annexin V-negative cells were necrotic cells (in the upper left quadrant: Q1). As anticipated, MCF-7 cells treated with both VPN (20 μM) and DOX (0.5 μM) in single as well as in combination regimen (VPN, 25 μM + DOX, 0.05 μM) for a duration of 24 h and 48 h resulted in significant increase of apoptotic cells compared to control untreated cells (Figure 8). The percentage of early apoptotic cells were measured to be 4.79%, 10.9%, 20.4% and late apoptotic cells were estimated to be 5.97%, 3.8%,16.9%, respectively with treatment of VPN and DOX in single as well as in combination regimen after 24 h of post-treatment. Parenthetically, a similar significantly high percentage of early apoptotic cells of 12,5%, 14.1% and 21.3% as well as late apoptotic cells of 7.90%, 10.5% and 32.1%, respectively with treatment of VPN and DOX in single as well as in combination regimen, after 48 h, was measured and compared to controlled untreated cells (Figure 8). The control untreated cell culture contained only very few early apoptotic (0.83% and 2.01% after 24 h and 48 h post-treatment) and late apoptotic cells (2.17% and 2.14% after 24 h and 48 h post-treatment), which were considered as the background cell death due to regular trauma during cell culture (Figure 8). This is mainly because we have taken unstained cell for gating

and put the stained control cells in the FACS analysis as per the standard protocol (Ji et al., 2017; Sivakumaran et al., 2018; Fan et al., 2018).

DAPI staining

The induction of apoptosis to cancer cells were observed under the inverted fluorescence microscope after treatment of VPN and DOX in single as well as in combination. The apoptotic cells have significant alteration in the membrane architecture, blebbing of plasma membrane, chromatin condensation and chromosomal breakdown (apoptotic bodies) which could be visualized using the 4′, 6-diamidino-2-phenylindole (DAPI) fluorescent dye. Both the compounds in both single and in combination, efficiently induced apoptosis to cancer cell as revealed in the (Figure 9).

Tryptophan quenching assay

Tubulin is autofluorescence due to presence of tryptophan amino acid. Thus any alteration in its conformation with ligand binding decreases emission fluorescence - a tool used to recognize a ligand binding. The reduced fluorescence intensity in presence of increasing concentration of VPN and DOX in single as well as in combination, indicates the binding of both the compounds with tubulin. The relative percentage of decrease in fluorescence intensity was 19.86% and 25.31% respectively in presence of 20 μM VPN and 0.5 μM of DOX and 55% in combination of DOX (0.05 μM) and VPN (25 μM) (Figure 10). The significant reduction in tubulin fluorescence intensity in the combine regimen of VPN and DOX indicate co-binding of both the ligands with tubulin.

ANS-binding assay (8-anilino-1-naphthalenesulfonic acid)

Next, we investigated the impact of VPN (20 and 50 μM) and DOX (0.5 μM) on tubulin conformation changes using ANS binding assay, a fluorescent probe that binds to the protein's hydrophobic patches. Treatment of tubulin with VPN (20 and 50 μM) showed increase in tubulin-ANS fluorescence intensity in a way dependent on the concentration (Figure 11). It showed 20% and 31.8% increase in fluorescence intensity at 20 and 50 μM of VPN, whereas 23.39% in presence of DOX (0.5 μM) in comparison to unbound tubulin. Similarly, the tubulin-ANS fluorescence intensity was increased to 45% in combination treatment of VPN (25 μM) and DOX (0.05 μM) as well as 54% in combination of VPN (50 μM) and DOX (0.05 μM). The relative increase in tubulin-ANS fluorescence intensity in combination treatment of VPN and DOX compared to single regimen indicates the synergistic effect in the binding of both the compounds onto their respective binding sites.

Conclusion

Our extensive molecular modelling, cellular and biochemical studies, revealed the combination effect of newly designed derivative of noscapine (VPN) and docetaxel. The calculated binding free energy with tubulin was found to be different when both the ligands bound together into their respective binding sites compared to their single binding. The molecular dynamic simulation for 100 ns also revealed stable interaction of both the ligands with the tubulin. The inhibition of proliferative activity was significantly enhanced when both the drugs were used for treatment together, compared to their single regimen treatment. Similarly, the combination regimen of VPN and DOX effectively interfered with the cell cycle progression and induced apoptosis to cancer cells compared to their single regimen treatment. Both the ligands also found to bind with tubulin efficiently at combination treatment. Taken together, it is concluded that the anticancer activity of both VPN and docetaxel could be combined for better therapeutic outcome with minimum toxicity. Thus the synergistic use of VPN and DOX could be a novel approach for the treatment of breast cancer.

Acknowledgements

We would like to acknowledge the financial support provided by the OHEPEE, Govt. of Odisha through World Bank. Shruti Gamya Dash wishes to acknowledge the award of student research fellowship (DST/INSPIRE/IF170022) by the Department of Science and Technology, Govt. of India. Further, we express our indebtedness to Dr. Manu Lopus, UM-DAE Centre for Excellence in Basic Sciences, Mumbai, for providing extended facilities. CSIR-IICT communication number: IICT/Pubs./2020/130.

Disclosure statement

No potential conflict of interest was reported by the authors.

References

Becke, A. D. (1993). A new mixing of Hartree-Fock and local density-functional theories. *The Journal of Chemical Physics*, *98*(2), 1372–1377. https://doi.org/10.1063/1.464304

Binkley, J. S., Pople, J. A., & Hehre, W. J. (1980). Self-consistent molecular orbital methods. 21. Small split-valence basis sets for first-row elements. *Journal of the American Chemical Society*, *102*(3), 939–947. https://doi.org/10.1021/ja00374a017

Bradford, M. M. (1976). A rapid and sensitive method for the quantitation of microgram quantities of protein utilizing the principle of protein-dye binding. *Analytical Biochemistry*, *72*, 248–254. https://doi.org/10.1006/abio.1976.9999

Case, D. A., Betz, R. M., Cerutti, D. S., Cheatham, T. E., III, Darden, T. A., Duke, R. E., Giese, T. J., Gohlke, H., Goetz, A. W., Homeyer, N., Izadi, S., Janowski, P., Kaus, J., Kovalenko, A., Lee, T. S., LeGrand, S., Li, P., Lin, C., Luchko, T., … Kollman, P. A. (2016). *AMBER 2016*. University of California.

Checchi, P. M., Nettles, J. H., Zhou, J., Snyder, J. P., & Joshi, H. C. (2003). Microtubule interacting drugs for cancer treatment. *Trends in Pharmacological Sciences*, *24*(7), 361–365. https://doi.org/10.1016/S0165-6147(03)00161-5

Chougule, M., Patel, A. R., Sachdeva, P., Jackson, T., & Singh, M. (2011). Anticancer activity of Noscapine, an opioid alkaloid in combination with Cisplatin in human non-small cell lung cancer. *Lung Cancer*, *71*(3), 271–282. https://doi.org/10.1016/j.lungcan.2010.06.002

Darden, T., York, D., & Pedersen, L. (1993). Particle mesh Ewald: An N. log (N) method for Ewald sums in large systems. *The Journal of Chemical Physics*, *98*(12), 10089–10092. https://doi.org/10.1063/1.464397

Essmann, U., Perera, L., Berkowitz, M. L., Darden, T., Lee, H., & Pedersen, L. G. (1995). A smooth particle mesh Ewald method. *The Journal of Chemical Physics*, *103*(19), 8577–8593. https://doi.org/10.1063/1.470117

Fan, B., Shi, S., Shen, X., Yang, X., Liu, N., Wu, G., Guo, X., & Huang, N. (2018). Effect of HMGN2 on proliferation and apoptosis of MCF-7 breast cancer cells. *Oncology Letters*, *17*(1), 1160–1166. https://doi.org/10.3892/ol.2018.9668

Friesner, R. A., Banks, J. L., Murphy, R. B., Halgren, T. A., Klicic, J. J., Mainz, D. T., Repasky, M. P., Knoll, E. H., Shelley, M., Perry, J. K., Shaw, D. E., Francis, P., & Shenkin, P. S. (2004). Glide: A new approach for rapid, accurate docking and scoring. 1. Method and assessment of docking accuracy. *Journal of Medicinal Chemistry*, *47*(7), 1739–1749. https://doi.org/10.1021/jm0306430

Gordon, M. S., Binkley, J. S., Pople, J. A., Pietro, W. J., & Hehre, W. J. (1982). Self-consistent molecular-orbital methods. 22. Small split valence basis sets for second-row elements. *Journal of the American Chemical Society*, *104*(10), 2797–2803. https://doi.org/10.1021/ja00374a017

Halgren, T. A., Murphy, R. B., Friesner, R. A., Beard, H. S., Frye, L. L., Pollard, W. T., & Banks, J. L. (2004). Glide: A new approach for rapid, accurate docking and scoring. 2. Enrichment factors in database screening. *Journal of Medicinal Chemistry*, *47*(7), 1750–1759. https://doi.org/10.1021/jm0306430

Hamel, E., & Lin, C. M. (1981). Glutamate-induced polymerization of tubulin: Characteristics of the reaction and application to the large scale purification of tubulin. *Archives of Biochemistry and Biophysics*, *209*(1), 29–40. https://doi.org/10.1016/0003-9861(81)90253-8

Hida, T., Kozaki, K., Ito, H., Miyaishi, O., Tatematsu, Y., Suzuki, T., Matsuo, K., Sugiura, T., Ogawa, M., Takahashi, T., & Takahashi, T. (2002). Significant growth inhibition of human lung cancer cells both *in vitro* and *in vivo* by the combined use of a selective cyclooxygenase 2 inhibitor, JTE-522, and conventional anticancer agents. *Clinical Cancer Research: An Official Journal of the American Association for Cancer Research*, *8*(7), 2443–2447.

Hida, T., Kozaki, K., Muramatsu, H., Masuda, A., Shimizu, S., Mitsudomi, T., Sugiura, T., Ogawa, M., & Takahashi, T. (2000). Cyclooxygenase 2 inhibitor induces apoptosis and enhances cytotoxicity of various anticancer agents in non small cell lung cancer cell lines. *Clinical Cancer Research: An Official Journal of the American Association for Cancer Research*, *6*(5), 2006–2011.

Jakalian, A., Jack, D. B., & Bayly, C. I. (2002). Fast, efficient generation of high-quality atomic charges. AM1-BCC model: II. Parameterization and validation. *Journal of Computational Chemistry*, *23*(16), 1623–1641. https://doi.org/10.1002/jcc.10128

Ji, Y., Yu, M., Qi, Z., Cui, D., Xin, G., Wang, B., Jia, W., & Chang, L. (2017). Study on apoptosis effect of human breast cancer cell MCF-7 induced by lycorine hydrochloride via death receptor pathway. *Saudi Pharmaceutical Journal: SPJ: The Official Publication of the Saudi Pharmaceutical Society*, *25*(4), 633–637. https://doi.org/10.1016/j.jsps.2017.04.036

Jordan, M. A., & Wilson, L. (2004). Microtubules as a target for anticancer drugs. *Nature Reviews Cancer*, *4*(4), 253–265. https://doi.org/10.1038/nrc1317

Jorgensen, W. L., Chandrasekhar, J., Madura, J. D., Impey, R. W., & Klein, M. L. (1983). Comparison of simple potential functions for simulating liquid water. *The Journal of Chemical Physics*, *79*(2), 926–935. https://doi.org/10.1063/1.445869

Kavanagh, J. J., & Kudelka, A. P. (1993). Systemic therapy for gynecologic cancer. *Current Opinion in Oncology*, *5*(5), 891–899. https://doi.org/10.1097/CAD.0000000000000057.

Kollman, P. A., Massova, I., Reyes, C., Kuhn, B., Huo, S., Chong, L., Lee, M., Lee, T., Duan, Y., Wang, W., Donini, O., Cieplak, P., Srinivasan, J., Case, D. A., & Cheatham, T. E. (2000). Calculating structures and free energies of complex molecules: Combining molecular mechanics and continuum models. *Accounts of Chemical Research*, *33*(12), 889–897. https://doi.org/10.1021/ar000033j

Lee, C., Yang, W., & Parr, R. G. (1988). Development of the Colle-Salvetti correlation-energy formula into a functional of the electron density. *Physical Review. B, Condensed Matter*, *37*(2), 785–789. https://doi.org/10.1103/physrevb.37.785

Mahaddalkar, T., Naik, P. K., Choudhary, S., Manchukonda, N., Kantevari, S., & Lopus, M. (2017). Structural investigations into the binding mode of a novel noscapine analogue, 9-(4-vinylphenyl) noscapine, with tubulin by biochemical analyses and molecular dynamic simulations. *Journal of Biomolecular Structure & Dynamics*, *35*(11), 2475–2484. https://doi.org/10.1080/07391102.2016.1222969

Maier, J. A., Martinez, C., Kasavajhala, K., Wickstrom, L., Hauser, K. E., & Simmerling, C. (2015). ff14SB: Improving the accuracy of protein side chain and backbone parameters from ff99SB. *Journal of Chemical Theory and Computation*, *11*(8), 3696–3713. https://doi.org/10.1021/acs.jctc.5b00255

Manchukonda, N. K., Naik, P. K., Sridhar, B., & Kantevari, S. (2014). Synthesis and biological evaluation of novel biaryl type α-noscapine congeners. *Bioorganic & Medicinal Chemistry Letters*, *24*(24), 5752–5575. https://doi.org/10.1016/j.bmcl.2014.10.046

Manchukonda, N. K., Naik, P. K., Santoshi, S., Lopus, M., Joseph, S., Sridhar, B., & Kantevari, S. (2013). Rational design, synthesis, and biological evaluation of third generation α-noscapine analogues as potent tubulin binding anti-cancer agents . *PLoS One*, *8*(10), e77970. https://doi.org/10.1371/journal.pone.0077970

Massova, I., & Kollman, P. A. (2000). Combined molecular mechanical and continuum solvent approach (MM-PBSA/GBSA) to predict ligand binding. *Perspectives in Drug Discovery and Design*, *18*(1), 113–135. https://doi.org/10.1023/A:1008763014207

Naik, P. K., Chatterji, B. P., Vangapandu, S. N., Aneja, R., Chandra, R., Kanteveri, S., & Joshi, H. C. (2011). Rational design, synthesis and biological evaluations of amino-noscapine: A high affinity tubulin-binding noscapinoid. *Journal of Computer-Aided Molecular Design*, *25*(5), 443–454. https://doi.org/10.1007/s10822-001-9430-4

Naik, P. K., Lopus, M., Aneja, R., Vangapandu, S. N., & Joshi, H. C. (2012). *In Silico* inspired design and synthesis of a novel tubulin-binding anticancer drug: Folate conjugated noscapine (Targetin). *Journal of Computer-Aided Molecular Design*, *26*(2), 233–247. Epub PMID: 22170255. https://doi.org/10.1007/s10822-011-9508-z

Naik, P. K., Santoshi, S., Rai, A., & Joshi, H. C. (2011). Molecular modelling and competition binding study of Br-noscapine and colchicine provide insight into noscapinoid-tubulin binding site. *Journal of Molecular Graphics & Modelling*, *29*(7), 947–955. https://doi.org/10.1016/j.jmgm.2011.03.004

Nawrocki, S. T., Sweeney-Gotsch, B., Takamori, R., & McConkey, D. J. (2004). The proteasome inhibitor bortezomib enhances the activity of docetaxel in orthotopic human pancreatic tumor xenografts. *Molecular Cancer Therapeutics*, *3*(1), 59–70.

Panda, D., Chakrabarti, G., Hudson, J., Pigg, K., Miller, H. P., Wilson, L., & Himes, R. H. (2000). Suppression of microtubule dynamic instability and treadmilling by deuterium oxide. *Journal of Biochemistry*, *39*(17), 5075–5081. https://doi.org/10.1021/bi992217f

Pietro, W. J., Francl, M. M., Hehre, W. J., Defrees, D. J., Pople, J. A., & Binkley, J. S. (1982). Self-consistent molecular orbital methods. 24. Supplemented small split-valence basis sets for second-row elements. *Journal of the American Chemical Society*, *104*(19), 5039–5048. https://doi.org/10.1021/ja00383a007

PTRAJ and CPPTRAJ. (2013). Software for Processing and Analysis of Molecular Dynamics Trajectory Data. *Journal of Chemical Theory and Computation*, *9*(7), 3084–3095. https://doi.org/10.1021/ct400341p.

Rowinsky, E. K. (1997). The development and clinical utility of the taxane class of antimicrotubule chemotherapy agents. *Annual Review of Medicine*, *48*, 353–374. https://doi.org/10.1146/annurev.med.48.1.353

Rowinsky, E. K., & Donehower, R. C. (1991). The clinical pharmacology and use of antimicrotubule agents in cancer chemotherapeutics. *Pharmacology & Therapeutics*, *52*(1), 35–84. https://doi.org/10.1016/0163-7258(91)90086-2

Ryckaert, J. P., Ciccotti, G., & Berendsen, H. J. (1977). Numerical integration of the cartesian equations of motion of a system with constraints: Molecular dynamics of *n*-alkanes. *Journal of Computational Physics*, *23*(3), 327–341. https://doi.org/10.1016/0021-9991(77)90098-5

Santoshi, S., Manchukonda, N. K., Suri, C., Sharma, M., Sridhar, B., Joseph, S., Lopus, M., Kantevari, S., Baitharu, I., & Naik, P. K. (2015). Rational design of biaryl pharmacophore inserted noscapine derivatives as potent tubulin binding anticancer agents. *Journal of Computer-Aided Molecular Design*, *29*(3), 249–270. https://doi.org/10.1007/s10822-014-9820-5

Santoshi, S., & Naik, P. K. (2014). Molecular insight of isotypes specific β-tubulin interaction of tubulin heterodimer with noscapinoids. *Journal of Computer-Aided Molecular Design*, *28*(7), 751–763. https://doi.org/10.1007/s10822-014-9756-9

Santoshi, S., Naik, P. K., & Joshi, H. C. (2011). Rational design of novel anti-microtubule agent (9-azido-noscapine) from quantitative structure activity relationship (QSAR) evaluation of noscapinoids. *Journal of Biomolecular Screening*, *16*(9), 1047–1058. https://doi.org/10.1177/1087057111418654

Shaik, M. S., Chatterjee, A., Jackson, T., & Singh, M. (2006). Enhancement of antitumor activity of docetaxel by celecoxib in lung tumors. *International Journal of Cancer*, *118*(2), 396–404. https://doi.org/10.1002/ijc.21325

Sivakumaran, N., Samarakoon, S. R., Adhikari, A., Ediriweera, M. K., Tennekoon, K. H., Malavige, N., Thabrew, I., & Shrestha, R. L. S. (2018). Cytotoxic and Apoptotic effects of Govaniadine isolated from *Corydalis govaniana* Wall. Roots on Human Breast Cancer (MCF-7) Cells. *BioMed Research International*, *2018*, 3171348. https://doi.org/10.1155/2018/3171348

Snyder, J. P., Nettles, J. H., Cornett, B., Downing, K. H., & Nogales, E. (2001). The binding conformation of Taxol in beta-tubulin: a model based on electron crystallographic density. *Proceedings of the National Academy of Sciences of the United States of America*, *98*(9), 5312–5316. https://doi.org/10.1073/pnas.051309398

Suri, C., Hendrickson, T. W., Joshi, H. C., & Naik, P. K. (2014). Molecular insight into γ-γ tubulin lateral interactions within the γ-tubulin ring complex (γ-TuRC). *Journal of Computer-Aided Molecular Design*, *28*(9), 961–972. https://doi.org/10.1007/s10822-014-9779-2

Suri, C., Joshi, H. C., & Naik, P. K. (2015). Molecular modeling reveals binding interface of γ-tubulin with GCP4 and interactions with noscapinoids. *Proteins: Structure, Function and Bioinformatics*, *83*(5), 827–843. https://doi.org/10.1002/prot.24773

Sweeney, C. J., Mehrotra, S., Sadaria, M. R., Kumar, S., Shortle, N. H., Roman, Y., Sheridan, C., Campbell, R. A., Murry, D. J., Badve, S., & Nakshatri, H. (2005). The sesquiterpene lactone parthenolide in combination with docetaxel reduces metastasis and improves survival in a xenograft model of breast cancer. *Molecular Cancer Therapeutics*, *4*(6), 1004–1012. https://doi.org/10.1158/1535-7163.MCT-05-0030

Theiss, C., & Meller, K. (2000). Taxol impairs anterograde axonal transport of microinjected horseradish peroxidase in dorsal root ganglia neurons *in vitro*. *Cell and Tissue Research*, *299*(2), 213–224. https://doi.org/10.1007/s004410050019

Topp, K. S., Tanner, K. D., & Levine, J. D. (2000). Damage to the cytoskeleton of large diameter sensory neurons and myelinated axons in vincristine-induced painful peripheral neuropathy in the rat. *The Journal of Comparative Neurology*, *424*(4), 563–576. https://doi.org/10.1002/1096-9861(20000904)424:4<563::AID-CNE1>3.0.CO;2-U

Wang, J., Wang, W., Kollman, P. A., & Case, D. A. (2006). Automatic atom type and bond type perception in molecular mechanical calculations. *Journal of Molecular Graphics & Modelling*, *25*(2), 247–260. https://doi.org/10.1016/j.jmgm.2005.12.005

Ye, K., Ke, Y., Keshava, N., Shanks, J., Kapp, J. A., Tekmal, R. R., Petros, J., & Joshi, H. C. (1998). Opium alkaloid noscapine is an antitumor agent that arrests metaphase and induces apoptosis in dividing cells. *Proceedings of the National Academy of Sciences of the United States of America*, *95*(4), 1601–1606. https://doi.org/10.1073/pnas.95.4.1601

Zhou, J., Gupta, K., Aggarwal, S., Aneja, R., Chandra, R., Panda, D., & Joshi, H. C. (2003). Brominated derivatives of noscapine are potent microtubule-interfering agents that perturb mitosis and inhibit cell proliferation. *Molecular Pharmacology*, *63*(4), 799–807. https://doi.org/10.1124/mol.63.4.799

Zhou, J., Liu, M., Luthra, R., Jones, J., Aneja, R., Chandra, R., Tekmal, R. R., & Joshi, H. C. (2005). EM012, a microtubule-interfering agent, inhibits the progression of multi drug-resistant human ovarian cancer both in cultured cells and in athymic nude mice. *Cancer Chemotherapy and Pharmacology*, *55*(5), 461–465. https://doi.org/10.1016/j.ejca.2010.02.017